

# RSC Advances



This is an *Accepted Manuscript*, which has been through the Royal Society of Chemistry peer review process and has been accepted for publication.

*Accepted Manuscripts* are published online shortly after acceptance, before technical editing, formatting and proof reading. Using this free service, authors can make their results available to the community, in citable form, before we publish the edited article. This *Accepted Manuscript* will be replaced by the edited, formatted and paginated article as soon as this is available.

You can find more information about *Accepted Manuscripts* in the [Information for Authors](#).

Please note that technical editing may introduce minor changes to the text and/or graphics, which may alter content. The journal's standard [Terms & Conditions](#) and the [Ethical guidelines](#) still apply. In no event shall the Royal Society of Chemistry be held responsible for any errors or omissions in this *Accepted Manuscript* or any consequences arising from the use of any information it contains.

Cite this: DOI: 10.1039/c0xx00000x

www.rsc.org/xxxxxx

# Highly effective oxygen reduction activity and durability of antimony-doped tin oxide modified PtPd/C electrocatalysts

Yuan Gao<sup>a,b</sup>, Ming Hou<sup>\*a</sup>, Zhigang Shao<sup>\*a</sup>, Changkun Zhang<sup>a,b</sup>, Xiaoping Qin<sup>a,b</sup> and Baolian Yi<sup>a</sup>

Received (in XXX, XXX) Xth XXXXXXXXX 20XX, Accepted Xth XXXXXXXXX 20XX

DOI: 10.1039/b000000x

## Abstract

Antimony-doped tin oxide (ATO) nanoparticles are synthesized by a simple one-step hydrothermal method. The oxygen reduction reaction (ORR) activity of the PtPd/C catalyst is promoted by the presence of ATO. Moreover, after accelerated durability testing, the PtPd/C-ATO catalyst reserves most of its electrochemically active surface area (ESA) and ORR activity compared to the PtPd/C catalyst. The improved electrochemical stability and activity of PtPd/C-ATO is attributed to the high stability of ATO support and the strong interaction between Pt and ATO.

## Introduction

Although proton exchange membrane fuel cells (PEMFCs) are ideal future power sources due to their high efficiency, zero emission, low-temperature operation, and fast response<sup>1</sup>, there are still some critical issues that need to be overcome before the commercialization of PEMFCs, which include the sluggish kinetics of the oxygen reduction reaction (ORR) and the unsatisfactory long-term durability of the cathode catalysts<sup>2,3</sup>. At present, the most widely used cathode catalyst system is Pt in the form of small nanoparticles supported on amorphous carbon particles. These carbon support materials can be oxidized when both oxygen and liquid water are present at high electrode potentials<sup>4,5</sup>, and when fuel hydrogen starvation occurs during fuel cell operation<sup>6-8</sup>. The electrochemical corrosion of the carbon support causes agglomeration and sintering of the Pt catalyst particles, resulting in a decreased electrochemical surface area (ESA) and deteriorative activity of the catalyst<sup>9</sup>. These effects would lead to a rapid degradation of the Pt catalyst and thus shorten the lifetime of the PEMFCs. Consequently, more robust catalysts with enhanced activity and stability, such as Pt-based alloy and core-shell catalysts have been studied as potential alternatives for PEMFCs<sup>10,11</sup>.

Carbon-supported PtPd catalysts with highly catalytic activity and long-term durability have received increasing interest for the application in ORR. The incorporation of Pd into Pt can modify its electronic state and reduce the local O coverage at high

potentials and thus stabilize the Pt surface due to separation and dilution of the active site<sup>12</sup>. To solve the carbon corrosion issue, alternative supports are being developed with the objectives to increase both the support durability and the catalyst activity through improving the catalyst-support interaction by replacing<sup>6,7,13-17</sup> or combining<sup>18,19</sup> carbon with transition metal oxides, such as antimony-doped tin oxide (ATO)<sup>20-27</sup>. Dou et al.<sup>20</sup> used ATO as catalyst support material for oxygen reduction reaction, and found that the ATO support maintains significantly its stability and the performance of the tested electrocatalyst compared to Vulcan XC-72. Furthermore, Yin et al.<sup>25</sup> proved that the electrochemical activity and stability of Pt for Pt/ATO/C catalysts is increased with the addition of ATO because of modified electronic structure of Pt by the presence of the ATO phase in the catalyst supports, which was found to significantly enhance the catalyst durability.

In this work, as an effort to improve the durability and activity of the catalysts, we developed a carbon-ATO composite support (abbreviated as C-ATO), and deposited PtPd catalyst on this support for oxygen reduction reaction. For comparison, PtPd supported on pure carbon support was also prepared. Their electrochemical performance and durability were evaluated, and the results are reported here.

## Experimental

### Material synthesis

The ATO nanoparticles were synthesized by a simple one-step hydrothermal method. Typically, 2 g tin (purity 99.99%) and calculated amount of Sb<sub>2</sub>O<sub>3</sub> (purity 99.99%) (5 at% to Sn) were dissolved in 80 mL 8.3 mol L<sup>-1</sup> HNO<sub>3</sub> solution and formed a yellow colloid. The colloid solution was transferred to an autoclave and kept at 150 °C for 10 h in an oven. When air cooled to room temperature, the resulting bluish-colored products (characteristic of ATO particle) were collected and washed with water and ethanol, and finally dried at 100 °C for 5 h in an oven.

<sup>a</sup>Fuel Cell System and Engineering Laboratory, Dalian Institute of Chemical Physics, Chinese Academy of Sciences, Dalian National Laboratory for Clean Energy, Dalian 116023, China.

Fax: +86-411-84379185; +86-411-84379153;

E-mail: zhgshao@dicp.ac.cn.

<sup>b</sup>University of Chinese Academy of Sciences, Beijing 100039, China. †

<sup>45</sup> Electronic Supplementary Information (ESI) available: [details of any supplementary information available should be included here]

12.3 c. See DOI: 10.1039/b000000x/

The C-ATO composite supports were prepared by mixing 13.6 mg ATO with 27.2 mg XC-72 in ethanol to obtain well-blended support suspensions.

The PtPd/C-ATO catalyst was prepared by a modified aqueous-phase synthesis method using amphiphilic triblock copolymers as the reductant and capping agent, according to Zhang et al.<sup>11</sup>. Typically, a given amount of Na<sub>2</sub>PdCl<sub>4</sub> (Aladdin, Shanghai, China) aqueous solution was injected into 14 g L<sup>-1</sup> Pluronic F127 (Sigma-Aldrich) solution to give a final PdCl<sub>4</sub><sup>2-</sup> concentration of 4.2 m mol L<sup>-1</sup>. After stirring at 80 °C for 2 h in an oil bath, the Pd colloid solution was obtained. Then calculated amount of Na<sub>2</sub>PtCl<sub>4</sub> (Aladdin, Shanghai, China) aqueous solution (Pd:Pt atom ratio of 2:1) was injected into the above solution, and kept at 80 °C for another 3 h to obtain PtPd nanocrystals (NCs). Afterwards, the as-prepared C-ATO support suspensions were added to the obtained PtPd NCs solution, then the mixture was stirred overnight. The product was collected by centrifugation and dried at 60 °C under vacuum overnight. For comparison, PtPd/C was also prepared by the same method with 40.8 mg XC-72 as support materials. The Pt/C and Pt/C-ATO were synthesized by removing the process of the Pd colloid formation from the preparation of PtPd/C and PtPd/C-ATO, respectively.

### Material characterizations

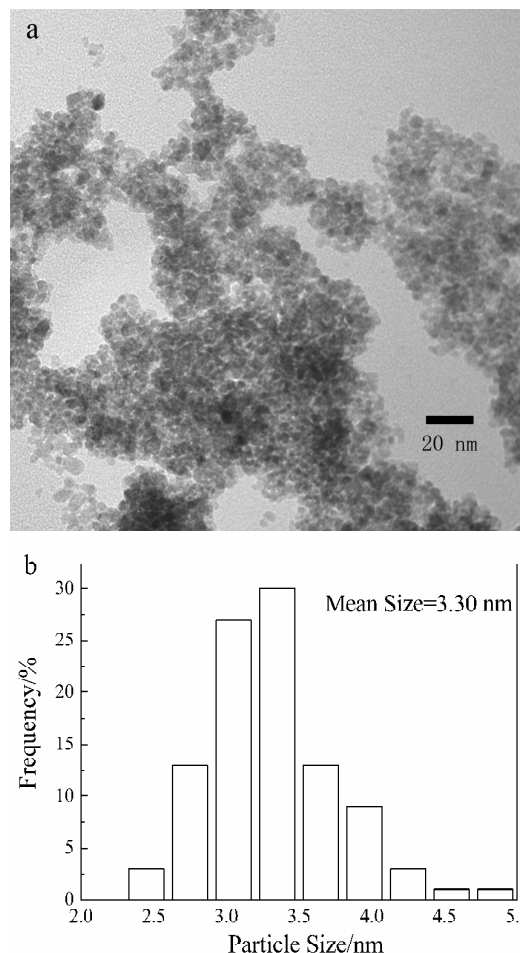
X-ray diffraction (XRD) measurements were carried out using a Cu K $\alpha$  source (PANalytical X'Pert PRO X-ray diffractometer) operated at 40 kV and 40 mA. Transmission electron microscope (TEM) characterization was performed on a JEOL JEM-2000EX microscope. The Brunauer-Emmet-Teller (BET) area was estimated using a QuadraSorb SI4 system. Elemental analysis was carried out on a JEOL 6360LV scanning electron microscopy equipped with an energy dispersive X-ray spectrometer (EDX). The XPS spectra were obtained on an ESCALAB250XI spectrometer and the binding energies were calibrated according to the C 1s peak (284.8 eV). The conductivities of support materials were tested using four-point probe measuring system (Suzhou Jingge Electronic Co., China).

### Electrochemical measurements

All electrochemical measurements were conducted using a CHI730 electrochemical station. Pt foil and saturated calomel electrode (SCE) were employed as the counter and reference electrode, respectively. All the potentials are given versus the normal hydrogen electrode (NHE). Working electrode was prepared by coating appropriate amount of electrocatalyst and Nafion® on the glassy carbon electrode (d = 4 mm) according to the literature<sup>28,29</sup>. Catalyst ink was obtained by sonicating 5 mg of catalyst, 50  $\mu$ L Nafion® solution (5 wt.%, Alfa Aesar), and 1 mL isopropanol into homogeneous slurry. Then, 4  $\mu$ L this ink was dropped on the glassy carbon electrode and allowed to dry in air at room temperature. All cyclic voltammetry (CV) measurements were profiled in 0.5 mol L<sup>-1</sup> H<sub>2</sub>SO<sub>4</sub> solution deaerated with high purity N<sub>2</sub> in the potential range of 0.02 and 1.2 V at a scan rate of 50 mV s<sup>-1</sup>. The oxygen reduction curve was measured in oxygen saturated 0.5 mol L<sup>-1</sup> H<sub>2</sub>SO<sub>4</sub> from 1.0 to 0.2 V at 10 mV s<sup>-1</sup> with a rotating speed of 1600 rpm. A potential cycling test from 0.6 V to 1.2 V were conducted to examine the electrochemical stability of the catalysts. The electrochemical surface area (ESA) of catalysts was estimated according to the charge of hydrogen desorption after double-layer correction, assuming monolayer hydrogen adsorption on Pt surface (0.21 mC cm<sup>-2</sup>).

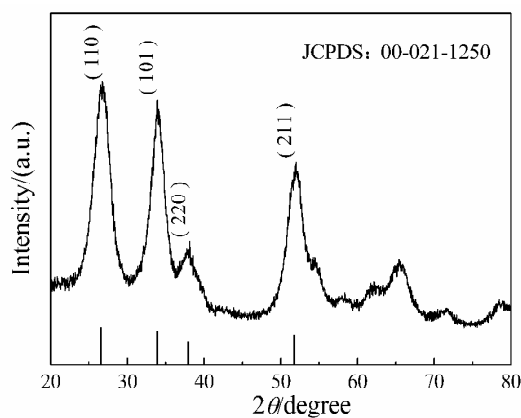
## Results and discussion

### Characterization of ATO Support Material



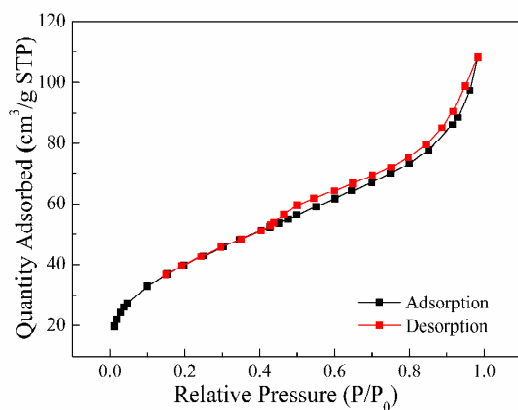
**Fig. 1** (a) TEM image and (b) corresponding particle size distribution histogram of ATO.

Figure 1a and 1b show TEM image and corresponding particle size distribution histogram of ATO. As seen from the TEM image, the ATO support material is composed of nanoparticles and has a relatively narrow particle size distribution. On the basis of measuring the size of more than 100 randomly chosen particles in the TEM image, the mean particle diameter of ATO support is 3.3 nm. Energy dispersive X-ray spectroscopy (EDX) analysis of the as-prepared support proved the presence of Sb and Sn in 5.4:100 atomic ratio for ATO, which agrees closely with the initial atomic ratio (5.0:100) used in ATO preparation.



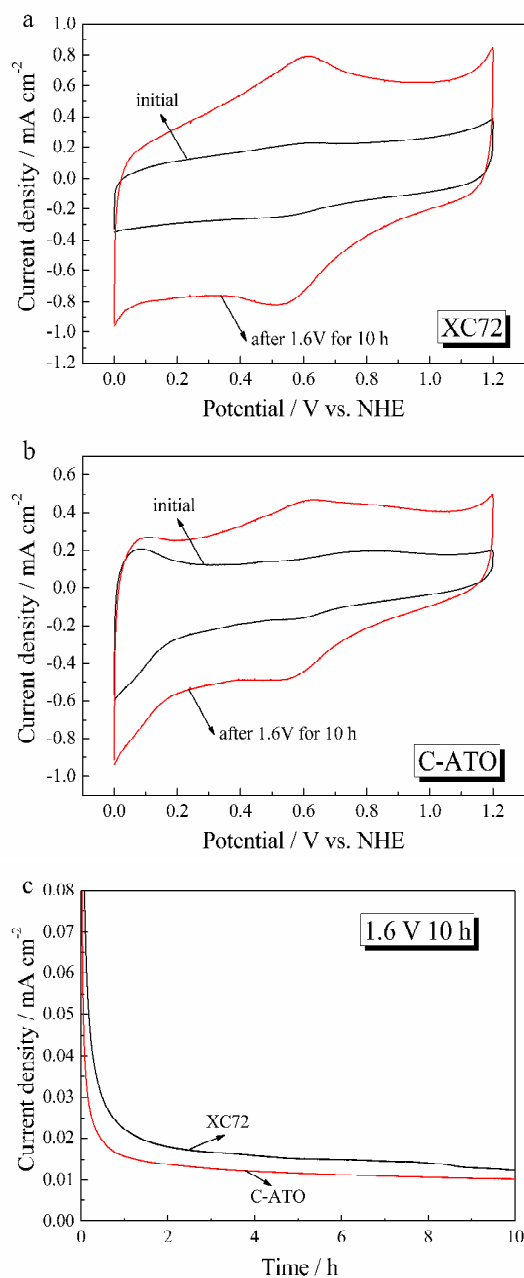
**Fig. 2** XRD pattern of ATO.

Figure 2 displays the XRD patterns of the ATO support material, all of the diffraction positions and relative intensities of support material match well with standard XRD pattern of cassiterite  $\text{SnO}_2$  (JCPDS card No. 00-021-1250). The main characteristic diffraction patterns at  $2\theta = 26.5, 33.8, 37.9,$  and  $51.7$ , correspond to the planes of (110), (101), (220), and (211), respectively. Moreover, there are no peaks arising from impurity, such as Sb,  $\text{Sb}_2\text{O}_3$  and  $\text{Sb}_2\text{O}_5$ . The average size of the ATO nanoparticles calculated from the (110) peak using Scherrer's equation is  $3.5$  nm, which is in accordance with the results obtained by TEM. Figure 3 exhibits the nitrogen adsorption/desorption isotherms of ATO support. As can be observed, the surface area of the ATO support synthesized in this study is found to be  $146.5 \text{ m}^2 \text{ g}^{-1}$ . In addition, the electronic conductivity of the ATO nanoparticles is measured as approximately  $1.47 \times 10^{-3} \text{ S cm}^{-1}$ .



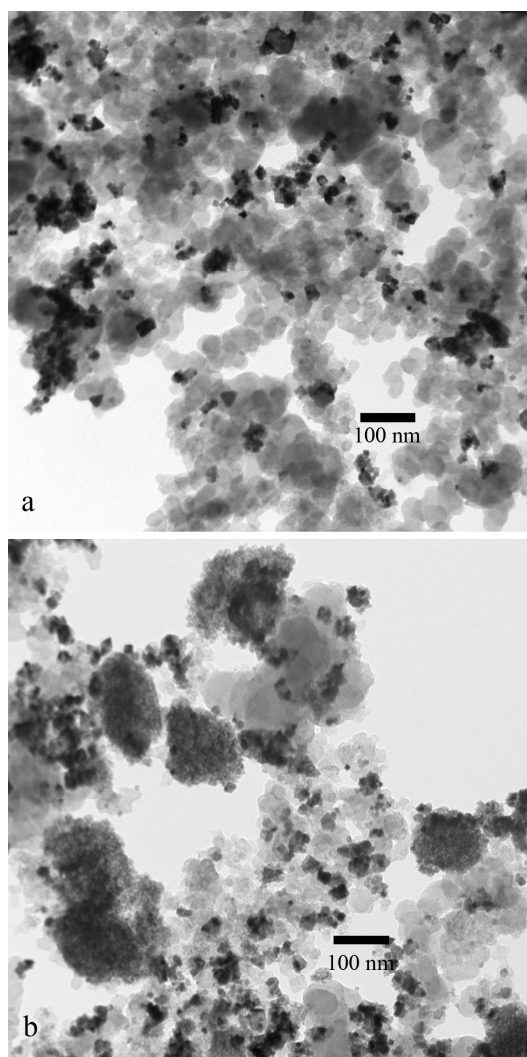
**Fig. 3** Nitrogen adsorption / desorption isotherms of ATO.

The electrochemical stabilities of XC-72 and C-ATO supports are studied by a rotating disk electrode (RDE) in  $0.5 \text{ mol L}^{-1} \text{ H}_2\text{SO}_4$  at an elevated potential. Figure 4a and 4b show the CV curves of XC-72 and C-ATO before and after potential hold at  $1.6 \text{ V}$  for  $10 \text{ h}$ . As seen in Figure 4a, the carbon support has a significant increase in the oxidation current after potential holding. The large redox couple at  $0.6 \text{ V}$  indicates that severe carbon corrosion has occurred. For C-ATO, there is still a redox couple at  $0.6 \text{ V}$  because of the presence of XC-72. However, the corrosion current of C-ATO after  $1.6 \text{ V}$  for  $10 \text{ h}$  is smaller than that of XC-72 (see Figure 4c), indicating that the prepared C-ATO composite support is rather more stable than commercial XC-72 carbon when subjected to high potentials.



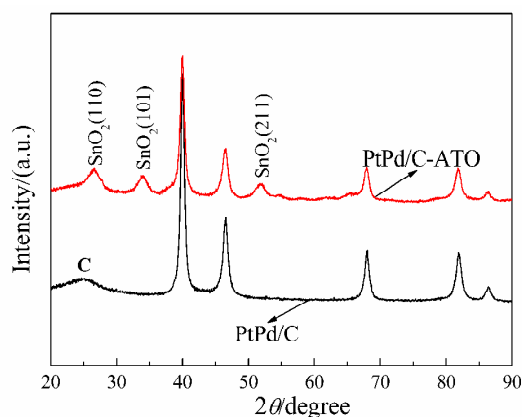
**Fig. 4** CV curves of XC-72 (a) and C-ATO (b) before and after  $1.6 \text{ V}$  oxidation for  $10 \text{ h}$  in  $0.5 \text{ mol L}^{-1} \text{ H}_2\text{SO}_4$  electrolyte with a scan rate of  $50 \text{ mV s}^{-1}$ ; (c) Chronoamperometric curves of XC-72 and C-ATO measured at  $1.6 \text{ V}$ .

#### 40 Characterization of the catalysts



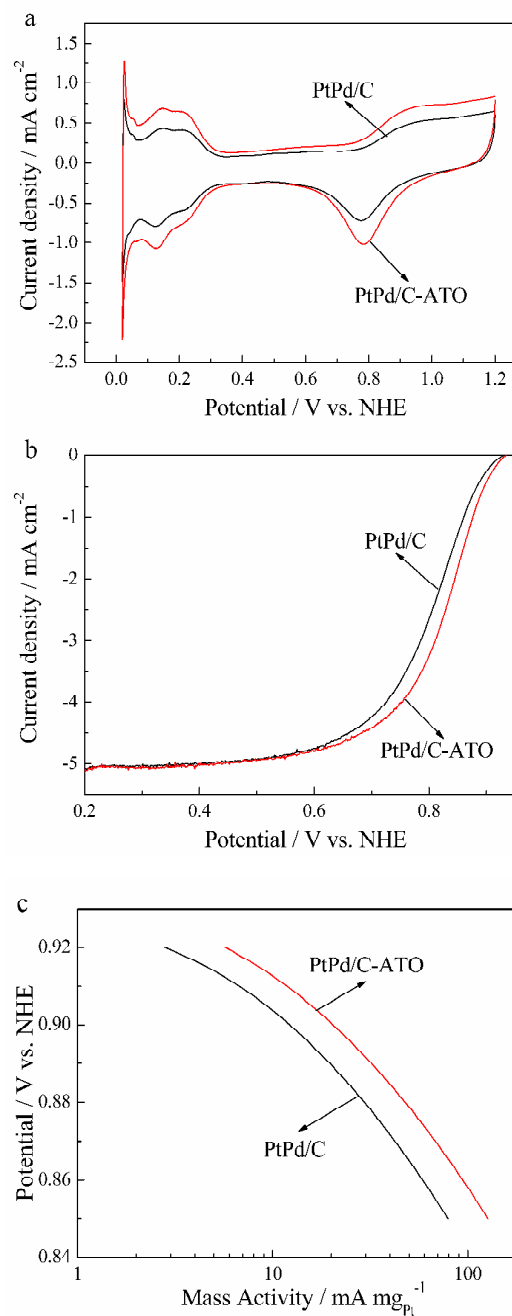
**Fig. 5** TEM images of PtPd/C (a) and PtPd/C-ATO (b).

Figure 5 displays the TEM images of PtPd/C and PtPd/C-ATO samples. For PtPd/C catalyst (Figure 5a), there are some irregular nanoparticles distributing on the carbon support. However, when ATO is added, the active component is distributing on both of the carbon support and the ATO support in the form of the clusters composed of nanoparticles (see Figure 5b).



**Fig. 6** XRD patterns of PtPd/C and PtPd/C-ATO.

The XRD patterns of PtPd/C and PtPd/C-ATO are shown in Figure 6. The diffraction peaks of the PtPd/C catalyst at around 40°, 47°, 68°, 81°, and 86° are attributed to the (111), (200), (220), (311) and (222) planes of the PtPd alloy (JCPDS card No. 03-065-6418), suggesting good crystallinity of these homemade PtPd NCs. The diffraction peak at around 25° comes from the carbon black. In terms of the PtPd/C-ATO catalyst, it can be seen that the catalyst displays characteristic peaks of PtPd crystalline structure, together with diffraction patterns of oxide component (ATO) with rutile SnO<sub>2</sub> structure which also can be found in Figure 2a. In addition, the mean crystallite size of PtPd NCs in each catalyst could be calculated by Scherrer's equation and found to be 12 and 11 nm for PtPd/C and PtPd/C-ATO catalysts, respectively.



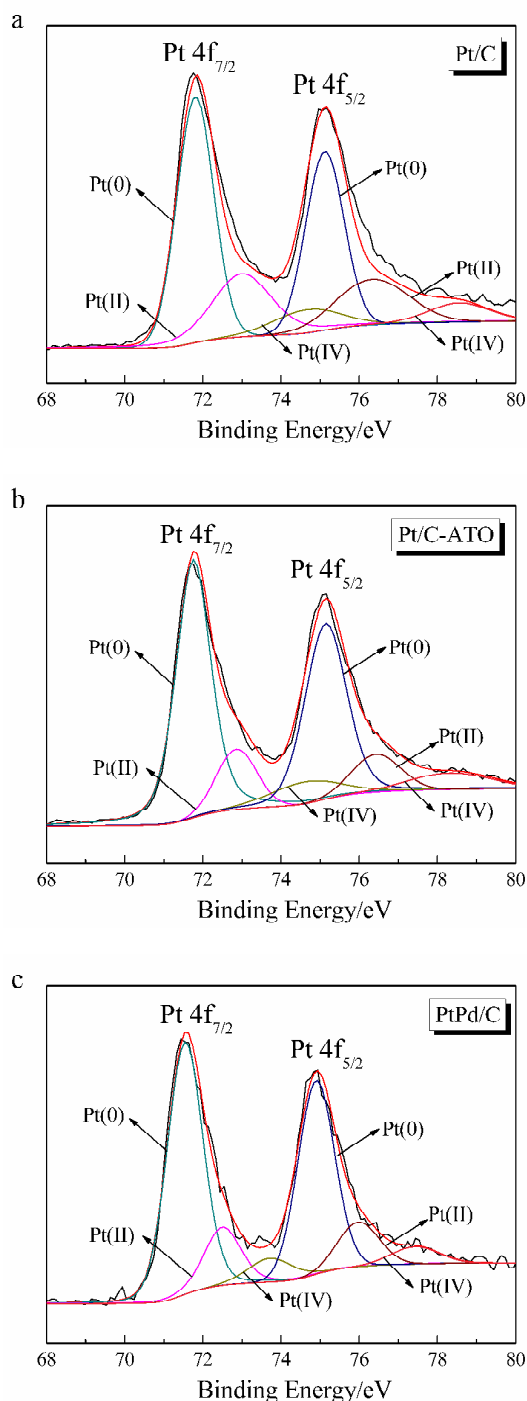
**Fig. 7** (a) CV curves, (b) ORR Polarization curves and (c) MA of PtPd/C and PtPd/C-ATO.

The electrocatalytic performances of PtPd/C and PtPd/C-ATO toward ORR are investigated in 0.5 mol L<sup>-1</sup> H<sub>2</sub>SO<sub>4</sub> at room temperature. The CV and ORR polarization curves for different catalysts are presented in Figure 7a and 7b. The Pt loading of PtPd/C and PtPd/C-ATO catalysts obtained by EDX are 13.49 wt.% and 14.23 wt.%, respectively. As seen from Figure 7a, the sharp peak, appeared between 0.02 and 0.05 V vs. NHE, may be ascribed to hydrogen absorption on Pd. The initial ESA, which is based on the Pt mass of the PtPd/C-ATO catalyst, is estimated to be 40.9 m<sup>2</sup> g<sup>-1</sup>, which is higher than that of the PtPd/C catalyst (27.5 m<sup>2</sup> g<sup>-1</sup>). The ORR polarization curves (Figure 7b) of the two catalysts show that the PtPd/C-ATO catalyst has more positive onset potential and half-wave potential than PtPd/C, which indicates the higher catalytic activity of PtPd/C-ATO than PtPd/C catalyst. The Pt mass activity (MA) (Figure 7c) is obtained by normalizing the kinetic current densities  $i_k$  against the Pt mass of these catalysts. The ORR mass activity of the PtPd/C-ATO catalyst at 0.9 V is 20.4 mA mg<sub>Pt</sub><sup>-1</sup>, higher than that of PtPd/C (12.2 mA mg<sub>Pt</sub><sup>-1</sup>).

**Table 1** Quantitative data of the fits of Pt 4f<sub>7/2</sub> XPS spectra for Pt/C, Pt/C-ATO, PtPd/C and PtPd/C-ATO.

Samples	BE of Pt (0)/eV	Values of Pt (0) in % in the total intensity
Pt/C	71.86	60.8
Pt/C-ATO	71.76	72.07
PtPd/C	71.54	73.29
PtPd/C-ATO	71.62	75.98

In order to understand the reason for an increase in the performance of the ORR activity by introduction of ATO, XPS analysis is conducted. Figure 8a, 8b, 8c and 8d show XPS spectra in Pt 4f region for Pt/C, Pt/C-ATO, PtPd/C and PtPd/C-ATO, respectively. The Pt4f peak in Figure 8 can be decomposed into pairs of three peaks, which are assignable to Pt (0), Pt (II) and Pt (IV) in each of the pairs. The binding energies (BE) of Pt4f<sub>7/2</sub> along with the relative densities of Pt (0) for each catalyst are listed in Table 1. As for the Pt/C-ATO catalyst, the BE of the Pt (0) is shifted to the lower energy with the addition of ATO on the support compared to the Pt/C catalyst. This result indicates the modulated interactions between Pt and supports by introduction of the ATO. In addition, the content of Pt (0) is found to be gradually increased from 60.18% for Pt/C to 72.07% for the Pt/C-ATO (see Table 1), further demonstrating the strong metal-support interactions between Pt and ATO. Similar results have also been observed by Yin et al.<sup>25</sup> In terms of the PtPd/C and PtPd/C-ATO catalysts, the BE of the Pt (0) for PtPd/C-ATO shifts positively by 0.08 eV compared to PtPd/C. The result is different from the shift of the BE between Pt/C and Pt/C-ATO. From XPS analysis, we can see that the surface Pt/Pd molar ratio of the PtPd/C catalyst is 0.65: 1. As for the PtPd/C-ATO, the surface Pt/Pd molar ratio is 0.57: 1. That is, when ATO is added, the surface Pt content decreases. Zhang et al.<sup>30</sup> suggest that the less Pt content in the surface of the catalyst, the more positive shift in the BE of the Pt in the Co@Pt/C catalysts. Therefore, the BE of the Pt (0) for PtPd/C shifts positively when ATO is added due to the less Pt content in the PtPd/C-ATO catalyst. Moreover, the content of Pt (0) for PtPd/C-ATO is 75.98%, higher than that of the PtPd/C (73.29%) (see Table 1). The result is similar to Liu et al.<sup>31</sup>, concluding that the content of Pt (0) in the PtAu/C increases with the addition of TiO<sub>2</sub>. Thus, the Pt in the PtPd/C-ATO possesses higher activity and stability due to the greater corrosion resistance of Pt (0).<sup>25</sup>



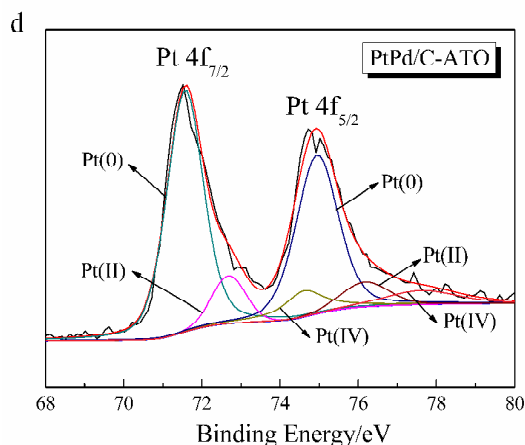


**Fig. 8** XPS spectra for Pt4f region of Pt/C (a), Pt/C-ATO (b), PtPd/C (c) and PtPd/C-ATO (d).

Furthermore, the long-term stability of PtPd/C and PtPd/C-ATO catalysts are evaluated by applying potential cycling between 0.6 and 1.2 V in  $N_2$ -purged  $0.5 \text{ mol L}^{-1} H_2SO_4$ , and the CV and ORR polarization curves before and after degradation are shown in Figure 9a, 9b, 9c and 9d. After 1500 cycles, the PtPd/C-ATO catalyst lost 67.5% of its initial Pt ESA, whereas the PtPd/C catalyst lost approximately 82.2% of its initial ESA. In addition, the mass activities of the two catalysts estimated from kinetic current densities versus the cycle number are shown in Figure 9c. As shown, the Pt mass activities of the PtPd/C and PtPd/C-ATO catalysts are enhanced in the first 100 potential cycles, which may be attributed to the compositional change of PtPd nanoalloy during potential cycling<sup>32</sup>. Some researches<sup>32, 33</sup> have reported that the non-noble metal in Pt-M alloy catalysts can be easily dissolved under electrochemical operating conditions, leaving the surface of the catalyst Pt-rich. Fig. 10 shows XPS spectra of the PtPd/C and PtPd/C-ATO catalysts before and after ADT in the binding energy ranges of Pd3d and Pt4f. It can be seen in Figure 10b that the Pd peaks of the PtPd/C and PtPd/C-ATO catalysts are decreased significantly, while the peak intensity of Pt (Figure 10a) reduces more slightly, suggesting remarkable Pd dissolution and little Pt loss after potential cycling. According to the intensity ratio of Pd3d and Pt4f, as derived from the area under the peaks, the Pd/Pt surface atomic ratio of the PtPd/C catalyst before ADT is evaluated to be 1.44: 1, while decreases to 0.84: 1 after ADT. The results indicate Pt enrichment on the outer layer. Similarly, the Pd/Pt surface atomic ratio of the PtPd/C-ATO catalyst after ADT (0.57: 1) is smaller than that of the PtPd/C-ATO catalyst before ADT (1.76: 1). The smaller lattice parameter of Pd-rich core would induce compressive strain in the outer shell, which would tend to downshift the d-band center of the Pt-rich shell<sup>34</sup>, weakening the adsorption energy of the oxygenated species, and thus enhancing the ORR kinetics of the dealloyed PtPd/C and PtPd/C-ATO catalysts<sup>35</sup>. Afterwards, the Pt mass activities for both of the catalysts are reduced during the potential cycling due to the significant decrease of ESA. The ORR activity of the PtPd/C-ATO catalyst at 0.9 V decreases to 54.4% of its initial value, while the PtPd/C catalyst retains only 39.4% of its initial ORR activity after 1500 cycles. Meanwhile, the ORR activity of the PtPd/C-ATO catalyst is 2.3 times higher than that of the PtPd/C catalyst after potential cycling. These results confirm that the PtPd/C-ATO catalyst is more durable than PtPd/C catalyst.

**Table 2** The mass activity (MA), specific activity (SA), electrochemical surface area (ESA), and decay rate of the PtPd/C and PtPd/C-ATO catalysts before and after potential cycling

between 0.6 and 1.2 V vs. NHE at  $50 \text{ mV s}^{-1}$  for 1500 cycles in  $50 N_2$ -purged  $0.5 \text{ mol L}^{-1} H_2SO_4$ .

Samples	ESA/ $m^2 g^{-1}$	MA/ $mA mg^{-1}$	SA/ $A m^{-2}$	
PtPd/C	0	27.5	12.2	1.0
	1500	4.9	4.8	0.98
	loss	82.2%	60.6%	2%
PtPd/C-ATO	0	40.9	20.4	0.5
	1500	13.3	11.1	0.83
	loss	67.5%	45.6%	-66%

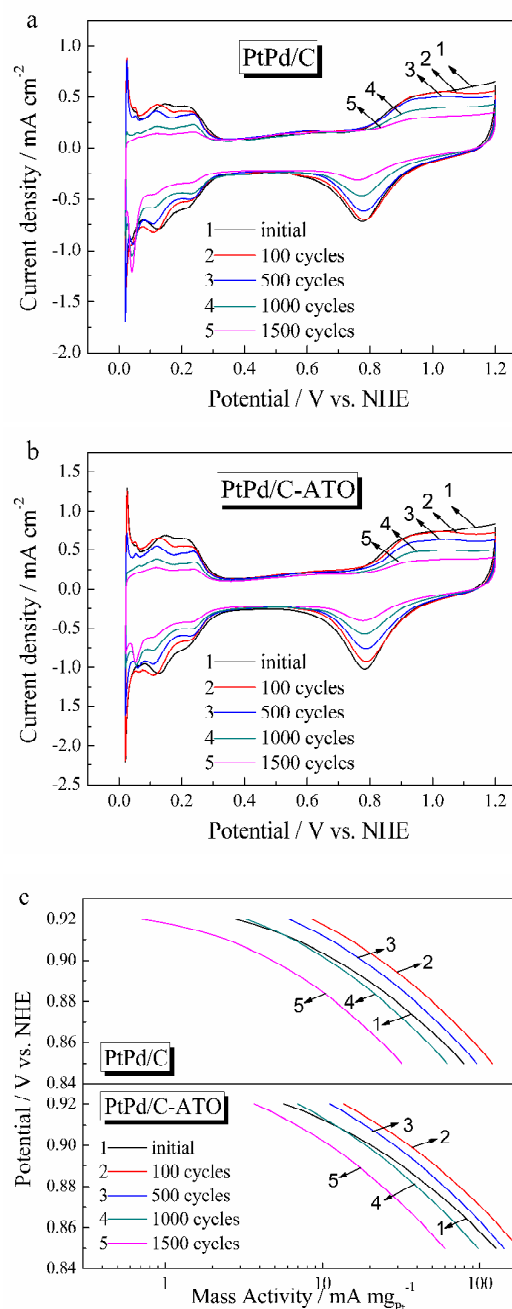


**Fig. 9** CV curves of (a) PtPd/C and (b) PtPd/C-ATO under 1500 potential cycling between 0.6 and 1.2 V; (c) MA given as kinetic current densities normalized against the Pt mass of PtPd/C and

PtPd/C-ATO as a function of cycle numbers; (d) Normalized mass activity as a function of cycle numbers for PtPd/C and PtPd/C-ATO.

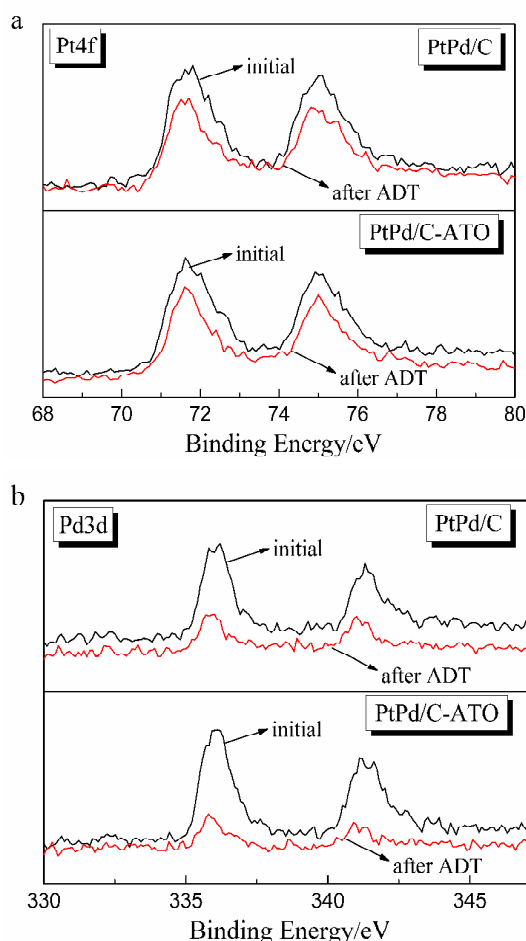


**Fig. 10** XPS spectra of the PtPd/C and PtPd/C-ATO catalysts before and after ADT in the binding energy ranges of (a) Pt4f and (b) Pd3d.

## Conclusions

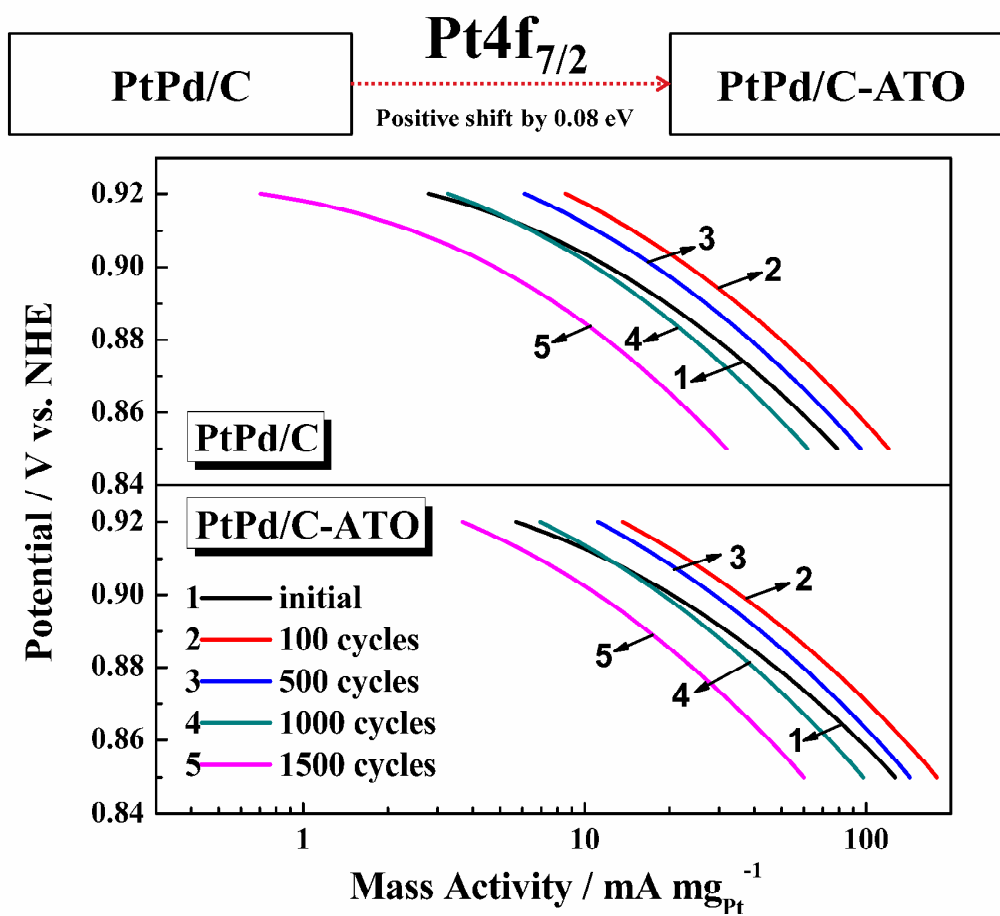
ATO nanoparticles with large surface area were successfully synthesized via a simple one-step hydrothermal method. The electrochemical stability of XC-72 improved when ATO was added. Meanwhile, the PtPd/C-ATO catalyst showed significantly enhanced catalytic activity for the ORR compared with the PtPd/C catalyst. The improvement of activity is attributed to the high ESA and modified electronic structure of Pt by the presence of the ATO phase in the catalyst supports which was also found to significantly enhance the catalyst durability.

## Acknowledgments

We gratefully acknowledge the financial support of this research by the National High Technology Research and Development Program (No. 2013AA110201) and the Key Project of Natural Science Foundation (No. 201436003).

## References

- N. Yousfi-Steiner, Ph. Mocot'eguy, D. Candusso, D. Hissel, A. Hernandez and A. Aslanides, *J Power Sources*, 2008, **183**, 260.
- R. Borup, J. Meyers, B. Pivovar, Y.S. Kim, R. Mukundan, N. Garland, D. Myers, M. Wilson, F. Garzon, D. Wood, P. Zelenay, K. More, K. Stroh, T. Zawodzinski, J. Boncella, J.E. McGrath, M. Inaba, K. Miyatake, M. Hori, K. Ota, Z. Ogumi, S. Miyata, A. Nishikata, Z. Siroma, Y. Uchimoto, K. Yasuda, K.-i. Kimijima and N. Iwashita, *Chem Rev*, 2007, **107**, 3904.
- M.K. Debe, *Nature*, 2012, **486**, 43.
- D.A. Stevens and J.R. Dahn, *Carbon*, 2005, **43**, 179.
- Y.-J. Wang, D.P. Wilkinson and J. Zhang, *Dalton Trans*, 2012, **41**, 1187.
- M. Dou, M. Hou, D. Liang, W. Lu, Z. Shao and B. Yi, *Electrochim Acta*, 2013, **92**, 468.
- M. Dou, M. Hou, H. Zhang, G. Li, W. Lu, Z. Wei, Z. Shao and B. Yi, *ChemSusChem*, 2012, **5**, 945.
- C.V. Subban, Q. Zhou, A. Hu, T.E. Moylan, F.T. Wagner and F.J. DiSalvo, *J Am Chem Soc*, 2010, **132**, 17531.
- V.T.T. Ho, C.-J. Pan, J. Rick, W.-N. Su and B.-J. Hwang, *J Am Chem Soc*, 2011, **133**, 11716.
- V.R. Stencovic, B. Fowler, B.S. Mun, G. Wang, P.N. Ross, C.A. Lucas and N.M. Markovic, *Science*, 2007, **315**, 493.
- G. Zhang, Z. Shao, W. Lu, H. Xiao, F. Xie, X. Qin, J. Li, F. Liu and B. Yi, *J Phys Chem C*, 2013, **117**, 13413.
- H. Li, G. Sun, N. Li, S. Sun, D. Su and Q. Xin, *J Phys Chem C*, 2007, **111**, 5605.
- C. Yao, F. Li, X. Li and D. Xia, *J Mater Chem*, 2012, **22**, 16560.
- C. Zhang, H. Yu, Y. Li, W. Song, B. Yi and Z. Shao, *Electrochim Acta*, 2012, **80**, 1.
- Y. Liu and W.E. Mustain, *J Am Chem Soc*, 2012, **135**, 530-533.
- S. Huang, P. Ganesan and B.N. Popov, *App Catal B-Environ*, 2011, **102**, 71.
- Y. Gao, M. Hou, Z. Shao, C. Zhang, X. Qin and B. Yi, *J Energy Chem*, 2014, **23**, 331.
- B. Ruiz-Camacho, J.H. Mart'nez-Gonzalez, R.G. Gonzalez-Huerta and M. Tufin'o-Velazquez, *Int J Hydrogen Energy*, 2014, **39**, 16731.
- N. Zhang, S. Zhang, C. Du, Z. Wang, Y. Shao, F. Kong, Y. Lin and G. Yin, *Electrochim Acta*, 2014, **117**, 413.
- M. Dou, M. Hou, F. Wang, D. Liang, Q. Zhao, Z. Shao and B. Yi, *J Electrochem Soc*, 2014, **161**, F1231.
- K.-S. Lee, I.-S. Park, Y.-H. Cho, D.-S. Jung, N. Jung, H.-Y. Park and Y.-E. Sung, *J Catal*, 2008, **258**, 143.
- M.P. Gurrola, M. Guerra-Balcázar, L. Álvarez-Contreras, R. Nava, J. Ledesma-García and L.G. Arriaga, *J Power Sources*, 2013, **243**, 826.
- K. Kakinuma, Y. Chino, Y. Senoo, M. Uchida, T. Kamino, H. Uchid, S. Deki and M. Watanabe, *Electrochim Acta*, 2013, **110**, 316.
- F. Takasaki, S. Matsuie, Y. Takabatake, Z. Noda, A. Hayashi, Y. Shiratori, K. Ito and K. Sasaki, *J Electrochem Soc*, 2011, **158**, B1270.
- M. Yin, J. Xu, Q. Li, J.O. Jensen, Y. Huang, L.N. Cleemann, N.J. Bjerrum and W. Xing, *App Catal B-Environ*, 2014, **144**, 112.
- C. Pan, Y. Li, Y. Ma, X. Zhao and Q. Zhang, *J Power Sources*, 2011, **196**, 6228.
- J. Xu, D. Aili, Q. Li, C. Pan, E. Christensen, J.O. Jensen, W. Zhang, G. Liu, X. Wang and N.J. Bjerrum, *J Mater Chem A*, 2013, **1**, 9737.
- U.A. Paulus, T.J. Schmidt, H.A. Gasteiger and R.J. Behm, *J Electroanal Chem*, 2001, **495**, 134.
- H.A. Gasteiger, S.S. Kocha, B. Sompalli and F.T. Wagner, *App Catal B-Environ*, 2005, **56**, 9.
- X. Zhang, H. Wang, J. Key, V. Linkov, S. Ji, X. Wang, Z. Lei and R. Wang, *J Electrochem Soc*, 2012, **159**, B270.
- C. Liu, H. Chen, C. Lai, J. Lin, L. Tsai and K. Wang, *ACS Appl Mater Interfaces*, 2014, **6**, 1589.
- W. He, H. Jiang, Y. Zhou, S. Yang, X. Xue, Z. Zou, X. Zhang, D.L. Akins and H. Yang, *Carbon*, 2012, **50**, 265.
- J. Zhao and A. Manthiram, *App Catal B-Environ*, 2011, **101**, 660.
- J. Zhang, Y. Mo, M.B. Vukmircovic, R. Klie, K. Sasaki and R.R. Adzic, *J Phys Chem B*, 2004, **108**, 10955.
- P. Strasser, S. Koh, T. Annyev, J. Greeley, K. More, C. Yu, Z. Liu, S. Kaya, D. Nordlund, H. Ogasawara, M. Toney and A. Nilsson, *Nat Chem*, 2010, **2**, 454.



The oxygen reduction reaction activity and stability of PtPd/C are promoted by introduction of antimony-doped tin oxide in the support.